Eigenmodes and resonance vibrations of graphene nanomembranes

Alexander V. Savin

N. N. Semenov Federal Research Center for Chemical Physics, Russian Academy of Sciences (FRCCP RAS), Moscow 119991, Russia and Plekhanov Russian University of Economics, Moscow 117997, Russia

(Received 19 February 2021; revised 12 May 2021; accepted 17 May 2021; published 24 May 2021)

Natural and resonant oscillations of suspended circular graphene membranes (single-layer sheets lying on a flat substrate having a circular hole of radius R) have been simulated using full-atomic models. Substrates formed by flat surfaces of graphite and hexagonal boron nitride (h-BN) crystal, hexagonal ice, silicon carbide 6H-SiC, and nickel (111) surface have been used. The presence of the substrate leads to the forming of a gap at the bottom of the frequency spectrum of transversal vibrations of the sheet. The frequencies of natural oscillations of the membrane (oscillations localized on the suspended section of the sheet) always lie in this gap, and the frequencies of oscillations decrease by increasing radius of the membrane as $(R + R_i)^{-2}$ with nonzero effective increase of radius $R_i > 0$. The modeling of the sheet dynamics has shown that small periodic transversal displacements of the substrate lead to resonant vibrations of the membranes at frequencies close to eigenfrequencies of nodeless vibrations of membranes with a circular symmetry. The energy distribution of resonant vibrations of the membrane has a circular symmetry and several nodal circles, whose number i coincides with the number of the resonant frequency. The resonant frequencies decrease with increasing the membrane radius as $(R + R_i)^{-\alpha_i}$ with the exponent $\alpha_i < 2$. The lower rate of resonance frequency decrease is caused by the hard anharmonicity of membrane vibrations.

DOI: 10.1103/PhysRevB.103.195435

I. INTRODUCTION

Being a nanosized polymorph of carbon, graphene attracts increased attention of researchers due to its unique physical properties [1,2]. The remarkable properties of graphene have enabled the exploitation of graphene for the development of nanoelectromechanical systems (NEMS) such as nanoresonators [3–5]. The vibrational properties of graphene play an important role in analysis and design of graphene-based sensors and resonators. The aim of this work is to simulate the eigenmodes and resonant vibrations of suspended circular graphene membranes. Such two-dimensional (2D) membranes are formed as single-layer graphene sheets lying on a flat substrate with a circular hole. These one-atom-thick membranes can be used as highly efficient nanomechanical resonators [6–15] and as extraordinary sensitive detectors of mass, force, and pressure [16–20]. A one-atom-thick layer of graphene sheet has very high Young's modulus, in-plane stiffness, and breaking strength [21]. It makes graphene membrane a promising candidate for ultrasensitive, low-power acoustic sensor.

Out-of-plane flexural modes play an important role in the mechanical [22], thermal [23,24], and electronic [25] properties of the graphene NEM resonators. The flexural modes of graphene membranes (resonators) have been studied in a continuum approximation (continuous thin plate or thin shell) [26–33] and in the framework of a lattice structure method [34,35]. These methods allow us to consider the vibrations of large-sized membranes with diameter $D > 10$ μm.

The molecular dynamics method requires significant computational resources and therefore allows studying the vibrations of only nanosize sheets [36–38], vibrations of membranes with diameter $D < 10$ nm.

The aim of this paper is to simulate the resonant vibrations of nanoscale circular graphene membranes. Previously, using the continuum approximation, only resonances of natural transverse vibrations of square graphene sheets with fixed edges were simulated [28,29]. Natural vibrations of a circular graphene membrane (of a circular piece with clamped edges) were considered in the continuous [26,33] and discrete (using the full-atomic model) [38] approximations.

In this paper, using the full-atomic model, natural vibrations and resonant transverse vibrations of a graphene sheet of size 15.6×15.6 nm^2 lying on a flat molecular substrate with a circular hole of radius $R \leqslant 6$ nm will be modeled (see Figs. 1 and 2). Let us note that this situation is realized in the experimental study of suspended graphene membranes [8,9,11,17]. As a substrate, we will consider flat surfaces of ideal graphite, hexagonal boron nitride (h-BN), hexagonal ice I_h, silicon carbide 6H-SiC, and the (111) surface of a nickel crystal.

The potential that describes the interaction of the graphene sheet with the substrate will be found and the natural flexural vibrations of the sheet (membrane) placed over the hole in the substrate will be analyzed. It will be shown that small amplitude periodic transversal displacements of the substrate lead to resonant vibrations of the membrane at frequencies close to eigenfrequencies of nodeless oscillations of membranes with a circular symmetry. The simulation of vibrations will be carried out taking into account the thermal vibrations of the membrane at a temperature of $T = 300$ K.

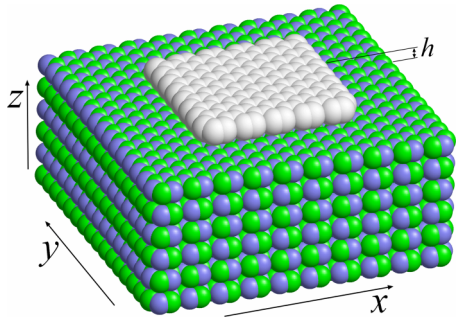

FIG. 1. Rectangular graphene sheet measuring 2.0×1.8 nm^2 (160 carbon atoms), lying parallel to the surface of h-BN crystal at distance h.

In Sec. II we describe the computational model, and in Sec. III the transverse normal modes of circular graphene membrane are analyzed. The effect of anharmonicity is addressed in Sec. IV, and Sec. V is devoted to the study of resonant vibrations. Our conclusions are presented in Sec. VI.

II. MODEL

To calculate the interaction energy of a graphene sheet with a flat substrate the sheet has been placed parallel to the substrate surface. The interaction potential of each atom belonging to the sheet with the substrate $W(h)$ can be found as the function of the distance to the substrate plane h, as a sum of its interaction energies with the substrate atoms. The interaction of pairs of atoms has been described by the Lennard-Jones (LJ) potential (6,12):

$$V_{\rm LJ}(r) = \epsilon_0[(r_0/r)^{12} - 2(r_0/r)^6], \qquad (1)$$

where ϵ_0 is the binding energy and r_0 is the bond length. To find the interaction energy of graphene with the crystalline graphite surface, we used the potential parameters taken from [39] and, for other substrates, from [40]. Table I shows the parameters of LJ potential (1) for various atomic pairs.

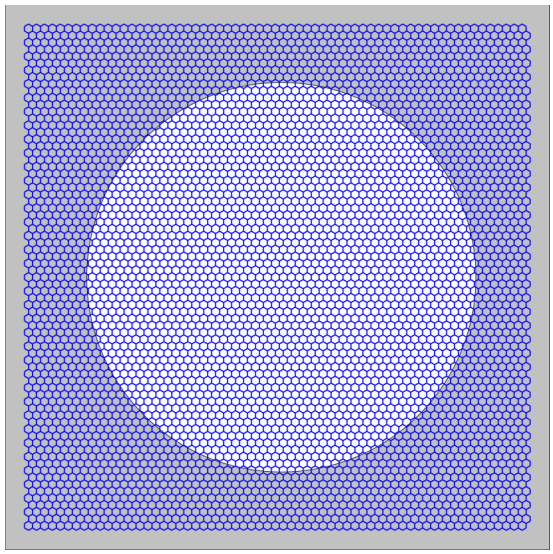

FIG. 2. The rectangular sheet of graphene lying on a flat substrate having a circular hole in its center. The sheet consists of 9470 carbon atoms and has the shape of a rectangle of size 15.6×15.6 nm^2. The radius of the hole in the substrate $R = 6$ nm.

TABLE I. Parameters of the LJ potential (1) for various pairs of interacting atoms.

	CC [39]	CC [40]	CH	CO	CSi	CN	CB
ϵ_0 (meV)	2.76	4.56	2.95	3.44	8.92	3.69	5.94
r_0 (Å)	3.809	3.851	3.369	3.676	4.073	3.754	3.965

The calculations have been made for the 2.0×1.8 nm^2 graphene sheet consisting of 160 carbon atoms, which is arranged in parallel to the crystal surface at distance h (see Fig. 1). At each value of distance h, the energy was averaged over the shifts along substrate surface and, then, normalized on the number of atoms in the graphene sheet. As a result, we obtained the dependence of the interaction energy of one atom of the sheet with the substrate on its distance from substrate plane $W(h)$. The calculations showed that the interaction energy with the substrate $W(h)$ can be described with a high accuracy by the Lennard-Jones potential (k, l):

$$W(h) = \epsilon_1[k(h_1/h)^l - l(h_1/h)^k]/(l-k), \qquad (2)$$

where power $l > k$. Potential (2) has the minimum $W(h_1) = -\epsilon_1$ (ϵ_1 is the binding energy of the atom with substrate). The stiffness of interaction with the substrate is $K_1 = W''(h_1) = \epsilon_1 lk/h_1^2$. Table II presents the parameters of LJ potential (2) for graphene sheet on various substrates.

When graphene is located on the (111) surface of crystalline nickel, a stronger chemical interaction of carbon atoms with the atoms of the substrate occurs (hybridization of the metal d band with graphene π states and charge transfer from the metal to graphene). As a result of the interaction of a graphene sheet with a crystal surface a gap of the magnitude $\omega_0 = 240$ cm^{-1} (1 cm^{-1} $= 2\pi \times 2.997925 \times 10^{10}$ s^{-1}) appears at the bottom of the frequency spectrum of transversal oscillations of the sheet [41]. From this we can estimate the harmonic coupling parameter of the interaction of the sheet atom with the substrate $K_1 = \omega_0^2 M_C = 41$ N/m (M_C is the mass of carbon atom). Therefore, for small displacements, the interaction with the substrate can be described by the harmonic potential

$$W(h) = \tfrac{1}{2}K_1(h - h_1)^2, \qquad (3)$$

with stiffness coefficient $K_1 = 41$ N/m and equilibrium distance to the substrate plane $h_1 = 2.145$ Å [42].

TABLE II. Parameters of (k, l) LJ potential (2) for graphene sheet on various substrates.

	ϵ_1 (eV)	h_1 (Å)	l	k	K_1 (N/m)
Graphene–Ice I$_h$	0.029	3.005	10	3.5	1.80
Graphene–Graphite	0.052	3.37	10	3.75	2.75
Graphene–6H-SiC	0.073	4.19	17	3.75	4.24
Graphene–h-BN	0.0903	3.46	10	3.75	4.53

To describe oscillations of the graphene sheet, we present the system Hamiltonian in the form

$$H = \sum_{n=1}^{N} \left[\frac{1}{2} M_n(\dot{\mathbf{u}}_n, \dot{\mathbf{u}}_n) + P_n + \delta_n W(z_n) \right], \tag{4}$$

where N is the number of atoms in the sheet, M_n is the mass of nth atom, $\mathbf{u}_n = (x_n(t), y_n(t), z_n(t))$ is the radius vector of nth atom at the time t. The term P_n describes the energy of interaction of the atom with index n with the neighboring atoms, term $W(z_n)$ the energy of interaction of the atom with substrate surface (the plane of the substrate coincides with the plane xy). Coefficient $\delta_n = 1$ if nth atom interacts and $\delta_n = 0$ if it does not interact with the substrate (if it lies above the hole in the substrate).

To describe the carbon-carbon valence interactions, let us use a standard set of molecular dynamics potentials [43,44]. We consider a hydrogen-terminated graphene sheet, where edge atoms correspond to the molecular group CH. We will consider such a group as a single effective particle at the location of the carbon atom. Therefore, in our model of graphene nanoribbons we take the mass of atoms inside the stripe as $M_n = M_C = 12m_p$, and for the edge atoms we consider a larger mass $M_n = M_C + M_H = 13m_p$ (where $m_p = 1.6603 \times 10^{-27}$ kg is the proton mass).

The valence bond between two neighboring carbon atoms n and k can be described by the Morse potential

$$U_1(\mathbf{u}_n, \mathbf{u}_k) = \epsilon_r \{\exp[-\alpha(r_{nk} - r_0)] - 1\}^2, \tag{5}$$

where $r_{nk} = |\mathbf{u}_n - \mathbf{u}_k|$, $\epsilon_r = 4.9632$ eV is the valence bond energy, and $r_0 = 1.418$ Å is the equilibrium valence bond length.

The valence angle deformation energy between three adjacent carbon atoms n, k, and l can be described by the potential

$$U_2(\mathbf{u}_n, \mathbf{u}_k, \mathbf{u}_l) = \epsilon_\varphi (\cos\varphi - \cos\varphi_0)^2, \tag{6}$$

where $\cos\varphi = (\mathbf{u}_n - \mathbf{u}_k, \mathbf{u}_l - \mathbf{u}_k)/r_{nk}r_{kl}$, and $\varphi_0 = 2\pi/3$ is the equilibrium valent angle. Parameters $\alpha = 1.7889$ Å^{-1} and $\epsilon_\varphi = 1.3143$ eV can be found from the small-amplitude oscillations spectrum of the graphene sheet [45]. Valence bonds between four adjacent carbon atoms n, m, k, and l constitute torsion angles, whose potential energy can be defined as

$$U_3(\phi) = \epsilon_\phi (1 - \cos\phi), \tag{7}$$

where ϕ is the corresponding torsion angle ($\phi = 0$ is the equilibrium value of the angle) and $\epsilon_\phi = 0.499$ eV.

A detailed discussion about the choice of the interatomic potential parameters can be found in [43]. The same set of potentials has been successfully used to simulate the heat transfer along the carbon nanotubes and nanoribbons [46] for the analysis of spatially localized oscillations [47–49] and also for the analysis of the theoretical strength and the postcritical behavior of deformed graphene [50,51].

If we want to simulate the absence of a substrate for a part of the sheet atoms, we must take $\delta_n = 0$ for these atoms. Figure 2 shows a square sheet of graphene of size 15.6×15.6 nm^2 consisting of $N = 9470$ carbon atoms. The central circular part of the sheet does not interact with the substrate (for atoms from this part the coefficient $\delta_n = 0$), forming a circular membrane of radius $R = 6$ nm.

III. TRANSVERSAL NORMAL MODES

Let us consider the transversal vibrations of the atoms of the sheet. The natural frequencies and normal modes were derived numerically as the solution of the problem on eigenvalues for matrices of the second derivatives of size $N \times N$.

When only transversal offsets are taken into account, the Hamiltonian of the sheet (4) can be written in the form

$$H = \tfrac{1}{2}(\mathbf{M}\dot{\mathbf{Z}}, \dot{\mathbf{Z}}) + \mathcal{P}(\mathbf{Z}), \tag{8}$$

where $\mathbf{M}$ is a diagonal matrix of all masses of the sheet, $\mathbf{Z} = \{z_n - h_0\}_{n=1}^N$ is N-dimensional vector of transversal displacements from equilibrium positions. Hamiltonian (8) corresponds to the equations of motion

$$-\mathbf{M}\ddot{\mathbf{Z}} = \frac{\partial}{\partial \mathbf{Z}} \mathcal{P}(\mathbf{Z}). \tag{9}$$

For small displacements, Eq. (9) reduces to a system of linear equations

$$-\mathbf{M}\ddot{\mathbf{Z}} = \mathbf{B}\mathbf{Z}, \tag{10}$$

where the matrix $\mathbf{B}$ has dimension $N \times N$,

$$\mathbf{B} = \left(\frac{\partial^2 \mathcal{P}}{\partial z_{n_1} \partial z_{n_2}} \bigg|_{\mathbf{Z}=\mathbf{0}} \right)_{n_1=1,n_2=1}^{N,N}.$$

Next, we make the transformation $\mathbf{Z} = \mathbf{M}^{-1/2}\mathbf{X}$, and reduce the system (10) to the linear equations of the form $-\ddot{\mathbf{X}} = \mathbf{C}\mathbf{X}$ with the symmetric matrix $\mathbf{C} = \mathbf{M}^{-1/2}\mathbf{B}\mathbf{M}^{-1/2}$. Solutions of this linear system describe the eigenmodes of the sheet oscillations, which can be presented in the form $\mathbf{X}(t) = A\mathbf{e}\exp(i\omega t)$, where A is the oscillation amplitude, $\omega = \sqrt{\lambda}$ is the frequency, λ and $\mathbf{e}$ are the eigenvalue and normalized eigenvector of the matrix $\mathbf{C}$ [$C\mathbf{e} = \lambda\mathbf{e}$, $(\mathbf{e}, \mathbf{e}) = 1$].

The eigenvalues of the matrix $\mathbf{C}$ can be found numerically. Numerical matrix diagonalization demonstrates that the presence of the substrate leads to the presence of the gap $[0, \omega_0)$ at the bottom of the frequency spectrum of transversal vibrations (minimum nonzero frequency $\omega_0 = \sqrt{K_1/M_C}$). All eigentransversal vibrations of the sheet with frequencies $\omega < \omega_0$ correspond to vibrations localized in the suspended central part of the sheet, i.e., to eigenvibrations of the circular membrane.

The dependence of the natural oscillations of the circular membrane on its radius is shown in Fig. 3. Here, frequency $\omega_0 = 78.87$ cm^{-1}. A graphene membrane on a crystalline h-BN substrate with a radius of the central hole in the substrate $R = 5$ has only one localized natural oscillation, at $R = 10$, 6 oscillations; at $R = 15$, 1; at $R = 20$, 23; at $R = 30$, 55; at $R = 40$, 94; at $R = 50$, 144; and at $R = 60$ Å, 209 natural oscillations. The minimum natural frequency of transversal vibrations of the membrane is approximated with high accuracy by the dependence

$$\omega_i \sim c_i (R + R_i)^{-2}, \tag{11}$$

with index $i = 1$, $c_1 = 3950$ cm^{-1} Å^2, $R_1 = 4.0$ Å.

Asymptotics (11) take place for all substrates, and this shows that the interaction of the sheet with the substrate leads to an additional increase in the effective radius of the membrane by R_i. The amount of additional increase depends on the force of interaction with the substrate. The stronger is the

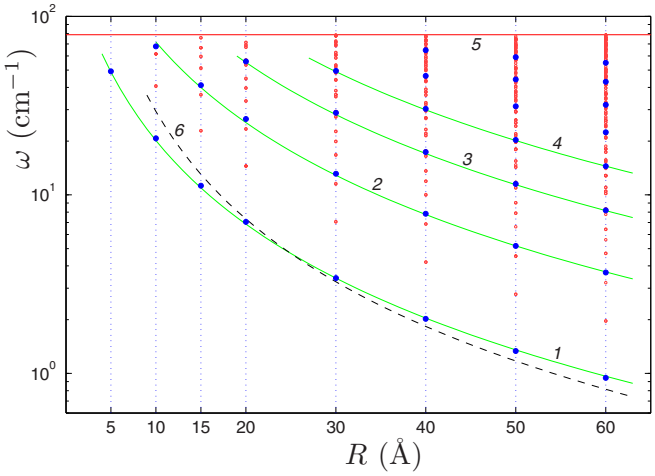

FIG. 3. Dependence of frequencies ω of intrinsic transversal oscillations of a circular membrane of a graphene sheet lying on the crystalline h-BN substrate on the radius of the membrane R. Curves $i = 1,\ 2,\ 3$, and 4 show the dependencies $\omega_i = c_i(R + R_i)^{-2}$, where coefficients $c_i = 3950$, 15 500, 34 500, and 62 500 cm^{-1}Å^2, and additional radius $R_i = 4.0$, 4.7, 5.0, and 5.7 Å. Straight line 5 shows the minimum frequency of transversal oscillations of a graphene sheet on a flat substrate $\omega = \omega_0 = 78.87$ cm^{-1}. Large blue markers show natural frequencies of intrinsic nodeless oscillations of the membrane with circular symmetry, while the small red markers stand for the other modes. The dashed curve 6 shows the dependence (12) obtained in [38].

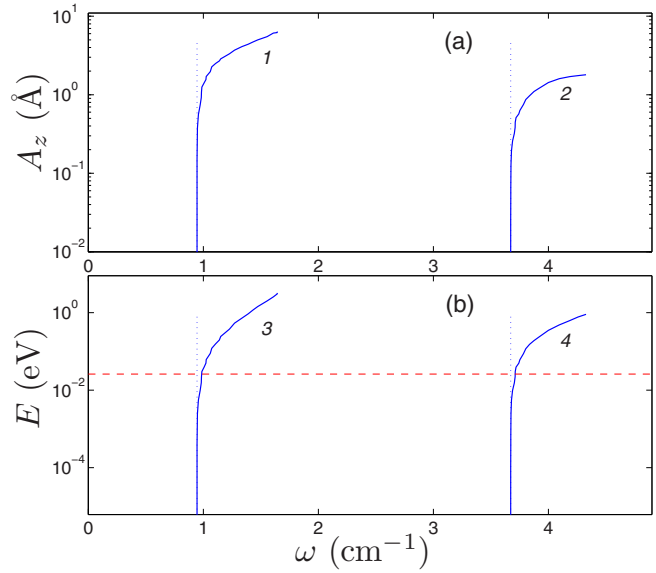

FIG. 4. Dependence of frequencies ω of the first and the second (curves 1, 3 and 2, 4) natural oscillations of the circular membrane ($R = 6$ nm) on (a) amplitude of transverse displacements of the membrane center A_z and (b) energy of vibration E. Energy of thermal vibrations $E = k_BT$ for temperature $T = 300$ K is represented by a horizontal dashed line.

interaction with the substrate, the smaller is the value of R_1. So $R_1 = 4.7$ for ice substrate having the weakest interaction with a sheet, $R_1 = 4.2$ for graphite substrate, $R_1 = 3.8$ for silicon carbide substrate, and $R_1 = 2.1$ Å for the Ni (111) substrate with the strongest interaction.

Higher-frequency natural nodeless oscillations of the membrane with circular symmetry also have asymptotic (11) with index $i = 2, 3, ...$(see Fig. 3).

Let us note that without taking into account the interaction with the substrate, the first frequency of a circular membrane with fixed edges is [38]

$$f_0 = \omega_0/2\pi = a/4R^2, \tag{12}$$

where $a = 3.52 \times 10^{-6}$ m^2/s. To obtain this dependence, the full-atom model of the membrane with REBO potential [52] was used. As can be seen in Fig. 3, both models show very close values of the first frequency ω_0.

IV. ANHARMONISM OF MEMBRANE VIBRATIONS

To simulate the natural vibrations of the membrane, we must numerically integrate a system of equations of motion

$$M_n\ddot{\mathbf{u}}_n = -\frac{\partial H}{\partial \mathbf{u}_n}, \quad n = 1, \ldots, N \tag{13}$$

with initial conditions

$$x_n(0) = x_n^0, \quad y_n(0) = y_n^0, \quad z_n(0) = z_n^0,$$
$$\dot{x}_n(0) = 0, \quad \dot{y}_n(0) = 0, \quad \dot{z}_n(0) = Ae_n,$$

where $\{\mathbf{u}_n^0 = (x_n^0, y_n^0, z_n^0)\}_{n=1}^N$ is the ground state of the graphene sheet, $\mathbf{e} = \{e_n\}_{n=1}^N$ is the eigenvector of the matrix $\mathbf{C}$ [amplitude A determines the energy of vibrations $E = A^2(\mathbf{Me}, \mathbf{e})/2$]. We will use the condition of absorbing edges (the friction $\Gamma = 1/t_r$ with time relaxation $t_r = 10$ ps was introduced at the edges of the sheet).

Let us consider the dynamics of the natural vibration of the membrane with radius $R = 60$ Å. Numerical integration of the system of equations of motion (9) has shown that when energy $E < E_0 = 0.01$ eV the membrane performs harmonic oscillations with eigenmode frequency (frequency of the vibration ω does not depend on the energy E). When $E > E_0$, the frequency of the membrane vibration begins to increase monotonically when increasing energy (see Fig. 4). Thus, at a high vibration energy, the membrane behaves like an anharmonic oscillator with hard anharmonicity. Let us note that at room temperature $T = 300$ K, the energy of thermal self-oscillation of the membrane $E > E_0$ ($E = k_BT = 0.026$ eV). Therefore, at room temperature, the thermal vibrations of the graphene membrane will be anharmonic.

V. RESONANT VIBRATIONS

To analyze the resonant vibrations of a single-layer membrane, we simulate the effect of forced periodic transverse motion of the substrate. To do this, we numerically integrate the system of Langevin equations of motion

$$M_n\ddot{x}_n = -\frac{\partial H}{\partial x_n} + \delta_n[-\Gamma M_n\dot{x}_n + \xi_{n,1}(t)],$$
$$M_n\ddot{y}_n = -\frac{\partial H}{\partial y_n} + \delta_n[-\Gamma M_n\dot{y}_n + \xi_{n,2}(t)], \tag{14}$$
$$M_n\ddot{z}_n = -\frac{\partial H}{\partial z_n} + \delta_n[-\Gamma M_n\dot{z}_n + \xi_{n,3}(t) + F(t, z_n)],$$

where the coefficient $\delta_n = 1$ if the atom interacts with the substrate and $\delta_n = 0$ if it does not interact (if it is located in the suspended part of the sheet), $\Gamma = 1/t_r$ is the friction coefficient, and random forces vectors $(\xi_{n,1}, \xi_{n,2}, \xi_{n,3})$ are normalized as follows:

$$\langle \xi_{n,i}(t_1)\xi_{m,j}(t_2)\rangle = 2M_n\Gamma k_B T\delta_{nm}\delta_{ij}\delta(t_1 - t_2),$$

where k_B is Boltzmann constant, T is temperature of the thermostat, and F is force of attraction of the atom to the substrate.

Let us note that the density of the air is more than 10^3 times less than the density of the substrate. The intensity of heat exchange with air will be approximately the same times less than the intensity of exchange with the substrate. Therefore, for nanosize graphene membrane we can neglect its heat interaction with the air.

If the position of the substrate plane is periodically changed along the z axis, then in the system of sheet motion equation (10) the force

$$F(t, z) = -W'[z + A\ \cos(\omega t)]$$

will be added, where A and ω are the amplitude and the frequency of the forced oscillations of the substrate. In order to illustrate better, we also define normalized amplitude $A_\omega = A\omega$ (by this definition the amplitude A_ω characterizes the oscillation energy, dimension $[A_\omega] = \text{Å}\,\text{cm}^{-1}$).

Let us analyze at what frequencies of forced oscillations of the substrate pumping of the energy to vibrations of the suspended section of the sheet will be the highest. For the sheet, the substrate is an external thermostat, so in the system of the equations of motion (14) only atoms in contact with the substrate interact with the Langevin thermostat. The intensity of heat exchange with the thermostat is characterized by a relaxation time t_r. The value $t_r = 1$ ps was used in the simulation. In the time $t_0 = 100t_r$ the sheet being fully thermalized. The analysis of the further dynamics of the sheet allows us to find the average temperature of the circular membrane

$$T_m = \frac{1}{3N_m k_B}\sum_{n=1}^{N}(1 - \delta_n)M_n\langle(\dot{\mathbf{u}}_n, \dot{\mathbf{u}}_n)\rangle,\ N_m$$
$$= \sum_{n=1}^{N}(1 - \delta_n),$$

where summation occurs only for atoms not in contact with the substrate (N_m is the number of such atoms), and the average value

$$\langle(\dot{\mathbf{u}}_n, \dot{\mathbf{u}}_n)\rangle = \lim_{t\to\infty}\frac{1}{t}\int_{t_0}^{t_0+t}(\dot{\mathbf{u}}_n(\tau), \dot{\mathbf{u}}_n(\tau))d\tau.$$

When the substrate is stationary (when the oscillation amplitude $A = 0$), the temperature of the membrane is always equal to the temperature of the thermostat ($T_m = T$). Therefore, additional thermalization of the membrane can be characterized by a temperature difference $\Delta T = T_m - T$.

Let us take the oscillation normalized amplitude $A_\omega = 1$ and 2 $\text{Å}\,\text{cm}^{-1}$, the temperature of the thermostat $T = 300$ K. The dependence of the additional thermalization of the membrane ΔT on the frequency of vertical oscillations of the substrate ω is shown in Fig. 5. As can be seen from the figure, the additional thermalization of the membrane is different from zero only near certain frequency values, the number of which increases with increasing membrane radius (see Fig. 6). Because by the vertical displacement of the substrate on all the edge atoms of the circular membrane are the same forces, the vertical vibrations of the substrate in the membrane can only cause vibrations with circular symmetry. Therefore, additional thermalization occurs only at frequencies close to the frequencies of the intrinsic nodeless oscillations of the membrane, which have a circular symmetry (the amplitude of the displacements of the membrane atom depends only on its distance from the center of the membrane). Thus, additional thermalization of the membrane occurs primarily due to the resonant pumping of its own circularly symmetric oscillations.

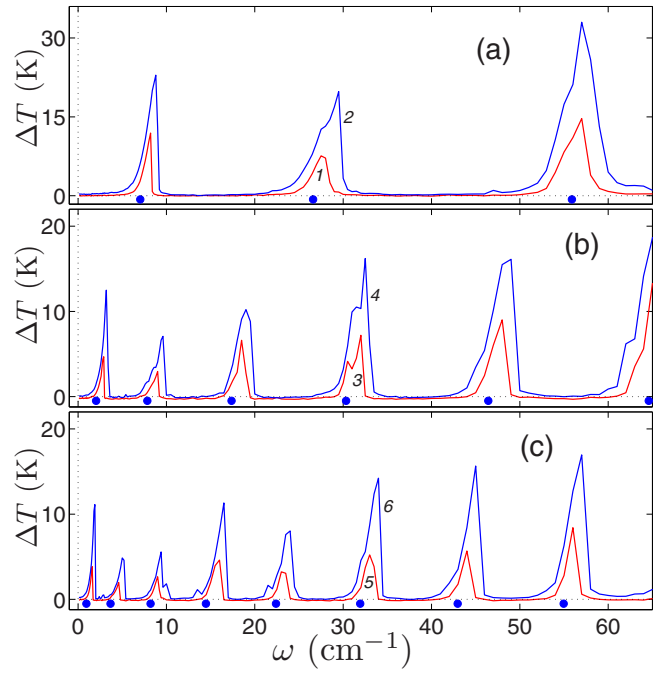

FIG. 5. Dependence of additional thermalization of the graphene membrane ΔT on the oscillation frequency of the h-BN substrate ω for membrane radius (a) $R = 2$, (b) $R = 4$, and (c) $R = 6$ nm. Red curves 1, 3, and 5 show dependencies for amplitude of forced substrate vibrations $A_\omega = 1$, blue curves 2, 4, and 6 dependencies for $A_\omega = 2$ $\text{Å}\,\text{cm}^{-1}$. The circular markers show the values of the frequencies of the intrinsic nodeless oscillations of the membrane with circular symmetry (see Sec. III and Fig. 3).

A similar resonant pumping of the membrane eigenmodes occurs for the graphene sheet for all considered substrates (see Fig. 6). As can be seen from the figure, the resonant pumping of the main oscillation occurs almost equally for all membranes. The differences appear only for higher frequency resonances. As the membrane radius increases, the resonance frequencies decrease and their number increases. The analysis of the energy distribution of resonant vibrations of the membrane (see Fig. 7) shows that the distribution always has a circular symmetry and has several nodal circles whose number coincides with the number of the resonance

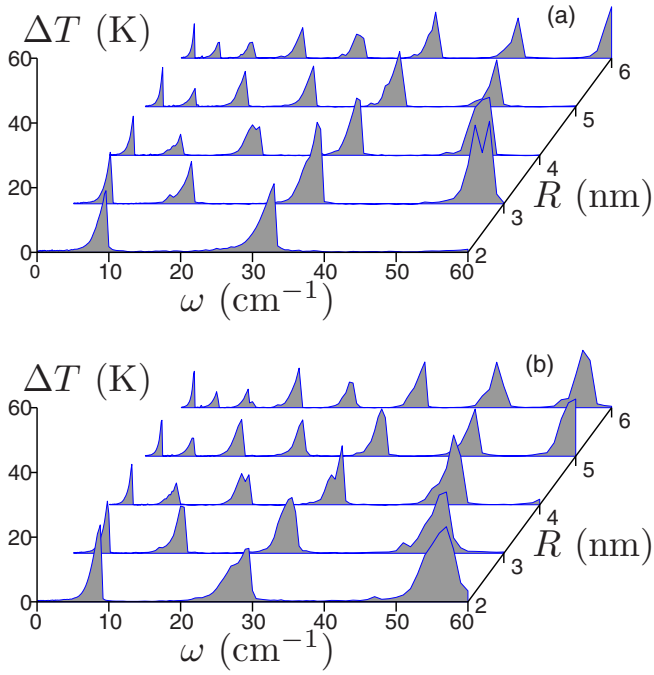

FIG. 6. Dependence of additional thermalization ΔT on the oscillation frequency of the substrate ω and on the membrane radius R for graphene membrane on substrates (a) Ni(111) and (b) 6H-SiC(0001) (normalized amplitude $A_\omega = 2$ Å cm^{-1}).

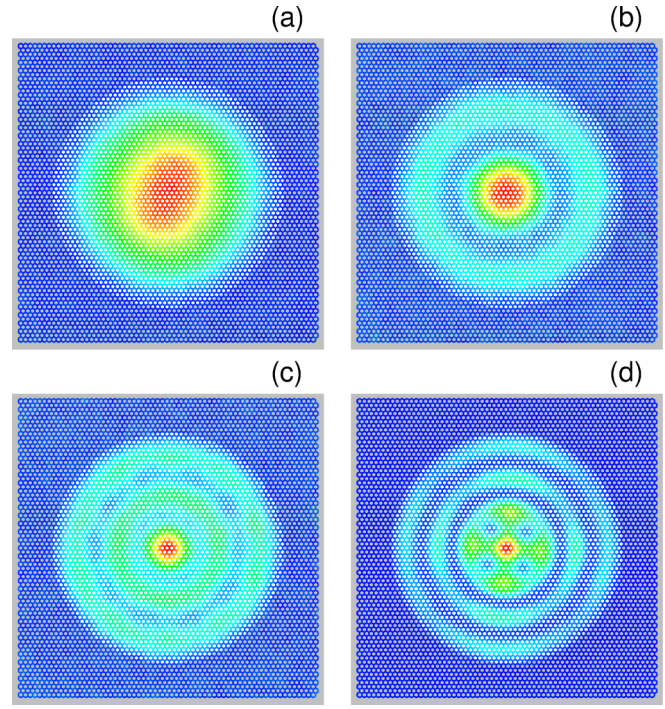

FIG. 7. Temperature distribution in a circular graphene membrane of radius $R = 6$ nm (h-BN substrate, normalized amplitude of forced substrate oscillations $A_\omega = 2$ Å cm^{-1}) at (a) first resonance (frequency $\omega = 1.9$ cm^{-1}, maximum temperature $T_m = 331$ K); (b) second resonance ($\omega = 5.0$ cm^{-1}, $T_m = 324$ K); (c) third resonance ($\omega = 9.4$ cm^{-1}, $T_m = 324$ K); (d) the fourth resonance ($\omega = 16.5$ cm^{-1}, $T_m = 366$ K). Blue color corresponds to the background temperature $T = 300$ K, red color corresponds to the maximum temperature T_m.

frequency. This shows that resonance pumping occurs primarily due to the excitation of natural oscillations of the membrane with circular symmetry (i.e., oscillations having only nodal circles).

Let us consider in more detail the first resonance of the membrane. As can be seen in Figs. 5 and 6, when the frequency increases, the vibrational energy of the membrane initially grows monotonically, at a certain frequency ω_r reaches its maximum value, and then sharply decreases to the background value of the energy of thermal vibrations. Therefore, it is convenient to determine the frequency of the first resonance as the average value

$$\bar{\omega}_1 = \frac{1}{C}\int_0^{1.1\omega_r} \omega \Delta T(\omega) d\omega, \quad C = \int_0^{1.1\omega_r} \Delta T(\omega) d\omega, \tag{15}$$

where ω_r is the first maximum of the function $\Delta T(\omega)$. Similarly, we can define the frequencies of next resonances $\bar{\omega}_i$, $i = 2, 3, \ldots$.

The results of numerical simulation of membrane vibrations are shown in Fig. 5. The figure shows that each ith eigenmembrane vibration with a circular (radial) symmetry corresponds to resonant membrane vibration with frequency $\bar{\omega}_i > \omega_i$. The resonance frequency is always higher than the frequency of the corresponding natural membrane vibration but lower than the frequency of the next natural vibration: $\omega_i < \bar{\omega}_i < \omega_{i+1}$, $i = 1, 2, 3, \ldots$. The larger the amplitude A of forced substrate vibration gets, the stronger the resonance frequency shifts to the right. This indicates the nonlinearity of resonances due to hard anharmonicity of membrane natural vibration at high energy (the frequency of natural vibration increases with increasing vibration amplitude). Let us note that the hard anharmonicity of graphene membrane was first experimentally detected in article [53] and then theoretically described in continuum membrane model [27].

The analysis of dependency of the resonance frequency $\bar{\omega}_i$ on membrane radius R shows that as the radius increases, the resonance frequency decreases slower than the frequency of the corresponding natural membrane vibration ω_i:

$$\bar{\omega}_i \sim d_i(R + R_i)^{-\alpha_i}, \quad \alpha_i < 2 \tag{16}$$

(see Fig. 8). The greater the amplitude A_ω of the substrate oscillation, the lower the value of exponent α_i. For the first resonance ($i = 1$) the exponent $\alpha_1 = 1.7$ for $A_\omega = 1$, and $\alpha_i = 1.6$ for $A_\omega = 2$ Å cm^{-1}. The deceleration of the decrease of the resonance frequencies $\bar{\omega}_i$ with increasing radius R is caused by the hard anharmonicity of the membrane vibrations. Hard anharmonicity of the membrane leads to a increase in the frequency of its transverse vibrations with an increase in their amplitude (see Fig. 4). In the asymptotics (16), this frequency increase is reflected in the decrease of the exponent α_i. For low-amplitude (harmonic) oscillations, the exponent is always equal 2 ($\alpha_i = 2$), for high-amplitude oscillations, the exponent monotonically decreases with increasing amplitude of the substrate oscillations ($\alpha_i \searrow$ for $A \nearrow$).

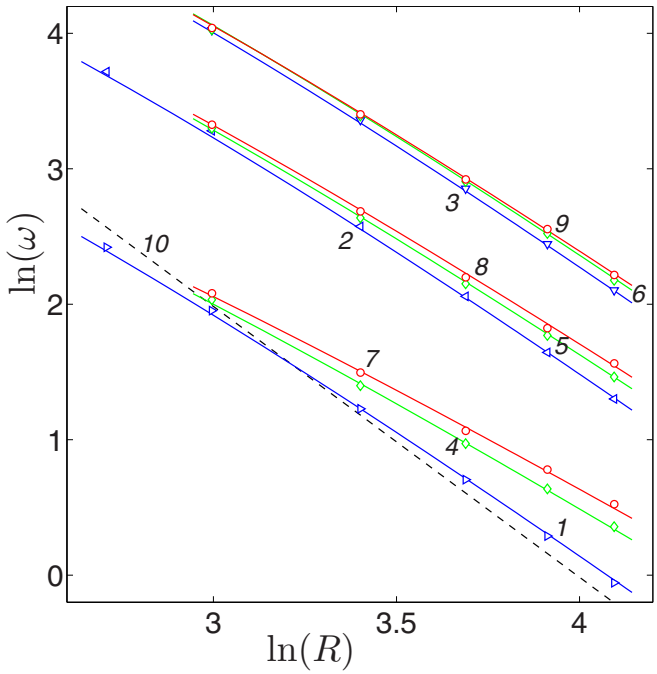

FIG. 8. Dependence of eigenoscillation frequencies ω_i ($i = 1$, 2, and 3, marked as 1, 2, and 3) and resonance frequencies $\bar{\omega}_i$ on membrane radius R (marked as 4, 5, 6 and 7, 8, 9 for normalized amplitude of forced substrate vibrations $A_\omega = 1$ and $A_\omega = 2$ Å cm^{-1}) for graphene on h-BN substrate. Blue curves 1, 2, 3 give approximations $\omega_i = c_i(R + R_i)^{-2}$ for $c_i = 3950$, 15 500, 34 500 cm^{-1} Å^2, $R_i = 4.0$, 4.7, 5.0 Å, $i = 1$, 2, 3. Green curves 4, 5, 6 give approximations $\bar{\omega}_i = d_i(R + R_i)^{-\alpha_i}$ for $A_\omega = 1$ ($d_i = 1650$, 11 900, 32 000, $\alpha_i = 1.7$, 1.9, 1.96), red curves 7, 8, 9 for $A_\omega = 2$ ($d_i = 1270$, 10 500, 2800 cm^{-1} Å$^{\alpha_i}$, $\alpha_i = 1.6$, 1.85, 1.92). The dashed line 6 shows the dependence (12) obtained in [38]. Dimension of the frequency $[\omega] =$ cm^{-1}, radius $[R] =$ Å.

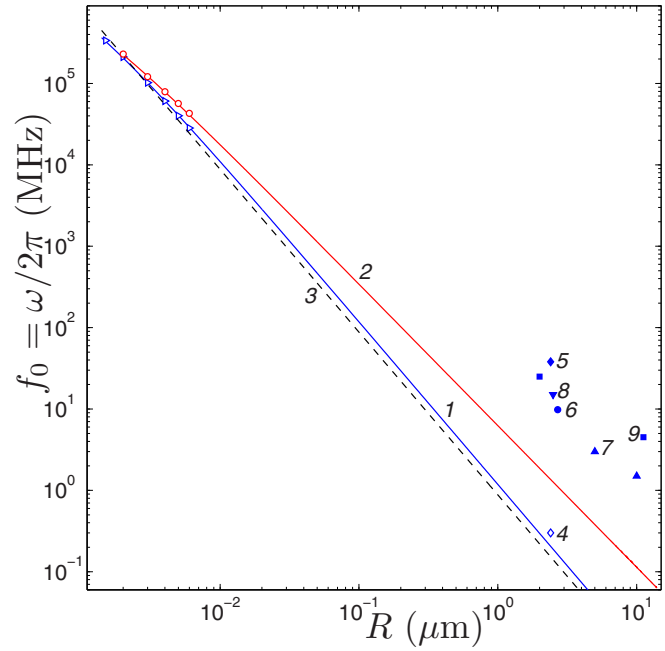

FIG. 9. Dependence of eigenoscillation frequencies ω_1 and resonance frequencies $\bar{\omega}_1$ on membrane radius R (curves 1 and 2) for normalized amplitude of forced substrate vibrations $A_\omega = 2$ Å cm^{-1}) for graphene on h-BN substrate. Blue curve 1 shows approximation $\omega_1 = c_1(R + R_1)^{-2}$ for $c_1 = 3950$ cm^{-1} Å^2, $R_1 = 4.0$. Red curve 2 shows approximations $\bar{\omega}_1 = d_1(R + R_1)^{-\alpha_1}$ for $A_\omega = 2$ ($d_1 =$ 1270 cm^{-1} Å$^{\alpha_1}$, $\alpha_1 = 1.6$. The dashed line 3 shows the dependence (12) obtained in [38]. Markers 4 and 5 show the values of the resonance frequencies of the unstressed and stressed membrane of radius $R = 2.4$ [17], marker 6 the value for membrane with $R = 2.7$ [11], 7 is the value for the membrane with $R = 5$, 10 [15], 8 for $R = 2.5$ [5], 9 for $R = 2$, 11.2; 8.566 μm [8].

The asymptotics for the eigenfrequencies and resonant frequencies of circular membranes (11) and (16) are obtained by simulating the vibrations of graphene membranes of radius $R \leqslant 6$ nm. It is clear that these asymptotics must also remain for membranes with a large radius. There are a number of experimental works on resonant vibrations of circular membranes with $R \geqslant 2$ μm [5,8,11,15,17]. Let us examine how the asymptotics applied for these membranes correlate with the frequency values obtained in these experimental works. The comparison of the asymptotics with the obtained values of the resonant frequencies is shown in Fig. 9. In [17], a single-layer graphene membrane with a diameter of $D = 4.8$ μm separating regions with different pressures was studied. In the absence of pressure (under zero tension), the main frequency of the membrane is $f_0 = 0.3$ MHz. As can be seen from the figure, this value corresponds well with the obtained asymptotics for the main eigenvibration of the membrane (11). At a pressure difference of $\Delta p = 93$ kPa, the membrane is already in a highly stressed (elongated) state, and its oscillation frequency increases significantly: $f_0 = 38$ MHz. As can be seen in Fig. 9, the experimental values of the resonant frequencies of circular single-layer graphene membranes are higher than the values of the predictable asymptotics (16). This can be explained by the fact that in the manufacture of membranes the graphene sheet covering the holes in the substrate remains in a stressed state.

VI. CONCLUSIONS

We have simulated natural and resonant oscillations of suspended circular graphene membranes using full-atomic models. The presence of the substrate [flat surface of graphite, h-BN crystal, hexagonal ice, silicon carbide 6H-SiC(0001), and (111) nickel surface] leads to the formation of a gap at the bottom of the frequency spectrum of transversal vibrations of the sheet. Frequencies of natural oscillations of the membrane ω_i always lie in this gap, and they decrease with the increasing radius of the membrane R as $(R + R_i)^{-2}$ with nonzero effective increase of radius $R_i > 0$. The modeling of the sheet dynamics has shown that forced small-amplitude periodic transversal vibrations of the substrate lead to resonant vibrations of the membranes, at frequencies close to the eigenfrequencies of nodeless vibrations of the membranes with circular symmetry. The energy distribution of the resonant vibrations of the membrane has a circular symmetry and several nodal circles whose number coincides with the number of the resonant frequency i. The frequencies of the

resonances decrease by increasing the radius of the membrane as $(R + R_i)^{-\alpha_i}$ with exponent $\alpha_i < 2$. The lower rate of the resonance frequency decrease is caused by the hard anharmonicity of membrane vibrations. Hard anharmonicity of the membrane leads to a increase in the frequency of its transverse vibrations with an increase in their amplitude.

ACKNOWLEDGMENTS

The author thanks Y. S. Kivshar for formulating this problem. The reported study was funded by RFBR, Project No. 18-29-19135. Computational facilities were provided by the Interdepartmental Supercomputer Center of the Russian Academy of Sciences.

[1] A. K. Geim and K. S. Novoselov, The rise of graphene, Nat. Mater. **6**, 183 (2007).
[2] C. Soldano, A. Mahmood, and E. Dujardin, Production, properties and potential of graphene, Carbon **48**, 2127 (2010).
[3] J. S. Bunch, A. M. van der Zande, S. S. Verbridge, I. W. Frank, D. M. Tanenbaum, J. M. Parpia, H. G. Craighead, and P. L. McEuen, Electromechanical resonatorsfrom graphene sheets, Science **315**, 490 (2007).
[4] K. Eom, H. S. Park, D. S. Yoon, and T. Kwon, Nanomechanical resonators and their applications in biological/chemical detection: Nanomechanics principles, Phys. Rep. **503**, 115 (2011).
[5] R. J. Dolleman, S. Houri, A. Chandrashekar, F. Alijani, H. S. J. van der Zant, and P. G. Steeneken, Opto-thermally excited multimode parametric resonance in graphene membranes, Sci. Rep. **8**, 9366 (2018).
[6] C. Chen, S. Rosenblatt, K. I. Bolotin, W. Kalb, P. Kim, I. Kymissis, H. L. Stormer, T. F. Heinz, and J. Hone, Performance of monolayer graphene nanomechanical resonators with electrical readout, Nat. Nanotechnol. **4**, 861 (2009).
[7] A. M. van der Zande, R. A. Barton, J. S. Alden, C. S. Ruiz-Vargas, W. S. Whitney, P. H. Q. Pham, J. Park, J. M. Parpia, H. G. Craighead, and P. L. McEuen, Large-scale arrays of single-layer graphene resonators, Nano Lett. **10**, 4869 (2010).
[8] R. A. Barton, B. Ilic, A. M. van der Zande, W. S. Whitney, P. L. McEuen, J. M. Parpia, and H. G. Craighead, High, size-dependent quality factor in an array of graphene mechanical resonators, Nano Lett. **11**, 1232 (2011).
[9] R. A. Barton, J. Parpia, and H. G. Craighead, Fabrication and performance of graphene nanoelectromechanical systems, J. Vac. Sci. Technol. B **29**, 050801 (2011).
[10] E. Grady, E. Mastropaolo, T. Chen, A. Bunting, and R. Cheung, Low frequency graphene resonators for acoustic sensing, Microelectron. Eng. **119**, 105 (2014).
[11] T. Inoue, Y. Anno, Y. Imakita, K. Takei, T. Arie, and S. Akita, Resonance control of a graphene drum resonator in a nonlinear regime by a standing wave of light, ACS Omega **2**, 5792 (2017).
[12] J. Güttinger, A. Noury, P. Weber, A. M. Eriksson, C. Lagoin, J. Moser, C. Eichler, A. Wallraff, A. Isacsson, and A. Bachtold, Energy-dependent path of dissipation in nanomechanical resonators, Nat. Nanotechnol. **12**, 631 (2017).
[13] G. J. Verbiest, J. N. Kirchhof, J. Sonntag, M. Goldsche, T. Khodkov, and C. Stampfer, Detecting ultrasound vibrations with graphene resonators, Nano Lett. **18**, 5132 (2018).
[14] M. Jung, P. Rickhaus, S. Zihlmann, A. Eichler, P. Makka, and C. Schönenberger, GHz nanomechanical resonator in an ultraclean suspended graphene p-n junction, Nanoscale **11**, 4355 (2019).
[15] S. A. Akbari, V. Ghafarinia, T. Larsen, M. M. Parmar, and L. G. Villanueva, Large suspended monolayer and bilayer graphene membranes with diameter up to 750 μm, Sci. Rep. **10**, 6426 (2020).
[16] A. Sakhaee-Pour, M. T. Ahmadian, and A. Vafai, Applications of single-layered graphene sheets as mass sensors and atomistic dust detectors, Solid State Commun. **145**, 168 (2008).
[17] J. S. Bunch, S. S. Verbridge, J. S. Alden, A. M. van der Zande, J. M. Parpia, H. G. Craighead, and P. L. McEuen, Impermeable atomic membranes from graphene sheets, Nano Lett. **8**, 2458 (2008).
[18] P. Weber, J. Güttinger, A. Noury, J. Vergara-Cruz, and A. Bachtold, Force sensitivity of multilayer graphene optomechanical devices, Nat. Commun. **7**, 12496 (2016).
[19] A. D. Smith, F. Niklaus, A. Paussa, S. Schröder, A. C. Fischer, M. Sterner, S. Wagner, S. Vaziri, F. Forsberg, D. Esseni, M. Östling, and M. C. Lemme, Piezoresistive properties of suspended graphene membranes under uniaxial and biaxial strain in nanoelectromechanical pressure sensors, ACS Nano **10**, 9879 (2016).
[20] D. Akinwande, C. J. Brennan, J. S. Bunch, P. Egberts, J. R. Felts, H. Gao, R. Huang, J.-S. Kim, T. Li, Y. Li, K. M. Liechti, N. Lu, H. S. Park, E. J. Reed, P. Wang, B. I. Yakobson, T. Zhang, Y.-W. Zhang, Y. Zhou, and Y. Zhu, A review on mechanics and mechanical properties of 2D materials—Graphene and beyond, Extreme Mech. Lett. **13**, 42 (2017).
[21] C. Chen and J. Hone, Graphene nanoelectromechanical systems, Proc. IEEE **101**, 1766 (2013).
[22] D. Midtvedt, A. Croy, A. Isacsson, Z. Qi, and H. S. Park, Fermi-Pasta-Ulam Physics with Nanomechanical Graphene Resonators: Intrinsic Relaxation and Thermalization from Flexural Mode Coupling, Phys. Rev. Lett. **112**, 145503 (2014).
[23] L. Lindsay, D. A. Broido, and N. Mingo, Flexural phonons and thermal transport in graphene, Phys. Rev. B **82**, 115427 (2010).
[24] Y. Wang, Z. Zhu, Y. Zhang, and L. Huang, Metastable states and energy flow pathway in square graphene resonators, Phys. Rev. E **97**, 012143 (2018).
[25] N. N. Klimov, S. Jung, S. Zhu, T. Li, C. A. Wright, S. D. Solares, D. B. Newell, N. B. Zhitenev, and J. A. Stroscio, Electromechanical properties of graphene drumheads, Science **336**, 1557 (2012).
[26] R. Ghaffari and R. A. Sauer, Modal analysis of graphene-based structures for large deformations, contact and material nonlinearities, J. Sound Vib. **423**, 161 (2018).
[27] E. Cadelano, P. L. Palla, S. Giordano, and L. Colombo, Nonlinear Elasticity of Monolayer Graphene, Phys. Rev. Lett. **102**, 235502 (2009).
[28] J. Atalaya, A. Isacsson, and J. M. Kinaret, Continuum elastic modeling of graphene resonators, Nano Lett. **8**, 4196 (2008).
[29] M. D. Dai, C.-W. Kim, and K. Eom, Nonlinear vibration behavior of graphene resonators and their applications in sensitive mass detection, Nanoscale Res. Lett. **7**, 499 (2012).
[30] A. M. Eriksson, D. Midtvedt, A. Croy, and A. Isacsson, Frequency tuning, nonlinearities and mode coupling in circular

mechanical graphene resonators, Nanotechnology **24**, 395702 (2013).

[31] S. Jiang, S. Shi, and X. Wang, Nanomechanics and vibration analysis of graphene sheets via a 2D plate model, J. Phys. D: Appl. Phys. **47**, 045104 (2014).

[32] J. R. Mianroodi, S. A. Niaki, R. Naghdabadi, and M. Asghari, Nonlinear membrane model for large amplitude vibration of single layer graphene sheets, Nanotechnology **22**, 305703 (2011).

[33] F.-T. Shi, S.-C. Fan, C. Li, and Z.-A. Li, Opto-thermally excited Fabry-Perot resonance frequency behaviors of clamped circular graphene membrane, Nanomaterials **9**, 563 (2019).

[34] A. Sakhaee-Pour, M. T. Ahmadian, and R. Naghdabadi, Vibrational analysis of single-layered graphene sheets, Nanotechnology **19**, 085702 (2008).

[35] S. Arghavan and A. V. Singh, Atomic lattice structure and continuum plate theories for the vibrational characteristics of graphenes, J. Appl. Phys. **110**, 084308 (2011).

[36] M. Sadeghi and R. Naghdabadi, Nonlinear vibrational analysis of single-layer graphene sheets, Nanotechnology **21**, 105705 (2010).

[37] S. O. Gajbhiye and S. P. Singh, Multiscale nonlinear frequency response analysis of single-layered graphene sheet under impulse and harmonic excitation using the atomistic finite element method, J. Phys. D: Appl. Phys. **48**, 145305 (2015).

[38] Y. Wang and L. Huang, Flexural modes of graphene resonators derived from the reactive empirical bond-order potential, Phys. Rev. B **101**, 195409 (2020).

[39] R. Setton, Carbon nanotubes. II. Cohesion and formation energy of cylindrical nanotubes, Carbon **34**, 69 (1996).

[40] A. K. Rappe, C. J. Casewit, K. S. Colwell, W. A. Goddard III, and W. M. Skiff, UFF, a full periodic table force field for molecular mechanics and molecular dynamics simulations, J. Am. Chem. Soc. **114**, 10024 (1992).

[41] A. Dahal and M. Batzill, Graphene-nickel interfaces: A review, Nanoscale **6**, 2548 (2014).

[42] Y. Gamo, A. Nagashima, M. Wakabayashi, M. Terai, and C. Oshima, Atomic structure of monolayer graphite formed on Ni(111), Surf. Sci. **374**, 61 (1997).

[43] A. V. Savin, Y. S. Kivshar, and B. Hu, Suppression of thermal conductivity in graphene nanoribbons with rough edges, Phys. Rev. B **82**, 195422 (2010).

[44] A. V. Savin and Y. S. Kivshar, Phononic Fano resonances in graphene nanoribbons with local defects, Sci. Rep. **7**, 4668 (2017).

[45] A. V. Savin and Y. S. Kivshar, Discrete breathers in carbon nanotubes, Europhys. Lett. **82**, 66002 (2008).

[46] A. V. Savin, B. Hu, and Y. S. Kivshar, Thermal conductivity of single-walled carbon nanotubes, Phys. Rev. B **80**, 195423 (2009).

[47] A. V. Savin and Y. S. Kivshar, Vibrational Tamm states at the edges of graphene nanoribbons, Phys. Rev. B **81**, 165418 (2010).

[48] E. A. Korznikova, A. V. Savin, Y. A. Baimova, S. V. Dmitriev, and R. R. Mulyukov, Discrete breather on the edge of the graphene sheet with the armchair orientation, JETP Lett. **96**, 222 (2012).

[49] J. A. Baimova, S. V. Dmitriev, and K. Zhou, Discrete breather clusters in strained graphene, Europhys. Lett. **100**, 36005 (2012).

[50] J. A. Baimova, S. V. Dmitriev, K. Zhou, and A. V. Savin, Unidirectional ripples in strained graphene nanoribbons with clamped edges at zero and finite temperatures, Phys. Rev. B **86**, 035427 (2012).

[51] E. A. Korznikova and S. V. Dmitriev, Moving wrinklon in graphene nanoribbons, J. Phys. D: Appl. Phys. **47**, 345307 (2014).

[52] S. J. Stuart, A. B. Tutein, and J. A. Harrison, A reactive potential for hydrocarbons with intermolecular interactions, J. Chem. Phys. **112**, 6472 (2000).

[53] C. Lee, X. Wei, J. W. Kysar, and J. Hone, Measurement of the elastic properties and intrinsic strength of monolayer graphene, Science **321**, 385 (2008).